Relative Strength of 4d vs 5d δ-Bonds: Rotational Barriers of Isostructural Molybdenum and Tungsten Porphyrin Dimers

James P. Collman,*,† J. Michael Garner,‡ Robert T. Hembre,§ and Yunkyoung Ha†

Contribution from the Departments of Chemistry, Stanford University, Stanford, California 94305, and University of Nebraska—Lincoln, Lincoln, Nebraska 68588-0304.
Received July 8, 1991

Abstract: Rotational barriers about the metal-metal quadruple bond axis in isostructural molybdenum ($\Delta G^{\ddagger}_{rot}$ = 10.8 ± 0.1 kcal/mol) and tungsten porphyrin dimers ($\Delta G^{\ddagger}_{rot}$ = 12.9 ± 0.1 kcal/mol) have been analyzed by variable-temperature dynamic NMR methods. As a measure of relative δ-bond strengths, these results indicate the tungsten δ-bond is 2.1 ± 0.5 kcal/mol stronger than the molybdenum δ-bond in the porphyrin system. A stronger tungsten δ-bond is consistent with the trend of increasing bond strengths to metals as one descends a column in the periodic table.

Introduction

The eclipsed geometry (D_{4h}) of both $ReCl_4$ fragments in the solid-state structure of $Re_2Cl_8^{2-}$ represented strong evidence for Cotton's proposal that quadruple bonds can exist between two metal atoms.[1] Consideration of ligand steric interactions alone would have predicted a staggered geometry (D_{4d}) to be more stable. The molecular orbital description for these bonds (Figure 1) explains this unexpected result by predicting the existence of a δ-bond between the rhenium atoms ($\sigma^2\pi^4\delta^2$). Like acetylenes, the σ- and degenerate π-components of quadruple bonds are axially symmetric and invariant with respect to rotation about the metal-metal axis. These bonds do not favor any rotational conformation. However, the δ-bond results from d_{xy}–d_{xy} overlap (z axis is the metal-metal bond) and depends on the relative orientation of each fragment. δ-Overlap is maximized in the perfectly eclipsed conformation but decreases to zero in the staggered. The observed geometry of $Re_2Cl_8^{2-}$ is then explained by assuming the δ-bond strength exceeds ligand-ligand repulsive forces in the eclipsed conformation.

Since this discovery, estimates for δ-bond strengths from theoretical studies and the analysis of spectroscopic properties have varied over a considerable range (100–0 kcal/mol),[1,2] but recent studies are in general agreement that the strengths are no more than 20 kcal/mol. Both of these methods for measuring δ-bond strengths suffer from the complexity and various assumptions inherent in these analyses. As a result, opinions vary as to the relative δ-bond strengths of different metals. Our interest in this problem led us to develop a more straightforward experimental approach to quantify δ-bond strengths. As described above, the qualitative MO scheme predicts these compounds should exhibit an *electronic barrier* to rotation about the metal-metal bond axis which is proportional to the δ-bond strength. With molybdenum porphyrin dimer derivatives, we measured such rotational barriers ($\Delta G^{\ddagger}_{rot}$ = 10.3 ± 0.5 kcal/mol) using variable-temperature NMR techniques and unequivocally demonstrated the ground-state rotational conformation was eclipsed.[4] These experiments represent unique solution evidence for quadruple bonding which compliments solid-state evidence.

But what is the relative δ-bond strengths of different metals? The recent discovery of efficient synthetic methods for tungsten porphyrin dimers[5] allowed a long-sought opportunity to answer this question for molybdenum and tungsten. In this paper, we report the measurement of these rotational barriers, the first *direct* comparison of the δ-bond *strengths* of second- and third-row metal dimers.

Results

As in the original δ-bond rotational barrier studies,[4] we employed a single meso substituent to break the characteristic 4-fold symmetry of octaethylporphyrin and divide the remaining meso protons into two which are adjacent to the substituent, H_{cis}, and one which is opposed, H_{trans} (Figure 2a). In the structural context of a metalloporphyrin dimer, this substitution generates five rotational isomers: three "eclipsed" (anti, gauche, and syn) and two "staggered" (anticlinal and synclinal) rotamers (Figure 3).[6] A primary issue in the analysis of a rotational barrier about a quadruple bond is the distinction between an eclipsed ground state, attributed to the electronic stabilization of the δ-bond, and a staggered ground state in which steric repulsions dominate.

In principle, this distinction may be established by ^1H NMR analysis: The three eclipsed rotamers contain seven symmetry-distinct meso protons (H_1–H_7; Figure 3a) while the two staggered rotamers contain a maximum of only six (H_1–H_6; Figure 3c). Observation of the individual NMR bands associated with each of these protons requires that the rate of rotation about the metal-metal bond, the exchange process, must be slow relative to the frequency difference of the bands ($k_{rot} < \omega_a - \omega_b$), referred to as the slow-exchange or slow-rotation regime. In the regime of rapid rotation ($k_{rot} > \omega_a - \omega_b$) both ground states give rise to two singlets for the meso bands with an H_{cis}:H_{trans} ratio of 2:1. Their chemical shifts ($\nu_{av} = \nu_{cis}$ or ν_{trans}) are population (P_m) weighted averages of the appropriate meso band from each rotamer observed in the slow-rotation regime (eq 1). As each ground-state rotamer contributes to H_{cis} and H_{trans}, not only the number of slow exchange meso bands but also the pattern of their convolution in the rapid exchange averaging process may distinguish an eclipsed from a staggered ground state (Figure 3b,d).

$$\nu_{av} = \sum P_m(\nu_n) \qquad (1)$$

† Stanford University.
‡ Present address: Du Pont Chemicals, E. I. du Pont de Nemours & Co., Wilmington, DE.
§ University of Nebraska—Lincoln.

(1) (a) Cotton, F. A.; Curtis, N. F.; Harris, C. B.; Johnson, B. F. G.; Lippard, S. J.; Mague, J. T.; Robinson, W. R.; Wood, J. S. *Science* **1964**, *145*, 1305–1307. (b) Cotton, F. A. *Inorg. Chem.* **1965**, *4*, 334–336. (c) Cotton, F. A.; Walton, R. A. *Multiple Bonds between Metal Atoms*; Wiley: New York, 1982; Chapter 1.

(2) Through an improved treatment of electron correlation,[3a-c] ab initio calculations have arrived at quadruple bond energies (85 ± 5 kcal/mol)[3d] for $Re_2Cl_8^{2-}$ in close agreement to experimental values (97 ± 12 kcal/mol).[3e] In addition, the theoretical δ-bond strength and rotational barrier obtained in these studies are in relatively good agreement with the experimental values for metalloporphyrin dimers herein.

(3) (a) Hay, P. J. *J. Am. Chem. Soc.* **1982**, *104*, 7007–7017. (b) Benard, M. *J. Am. Chem. Soc.* **1978**, *100*, 2354–2362. (c) Ziegler, T.; Tschinke, V.; Becke, A. *Polyhedron* **1987**, *6*, 685–693. (d) Smith, D. C.; Goddard, W. A., III *J. Am. Chem. Soc.* **1987**, *109*, 5580–5583. (e) Morss, L. R.; Porcja, R. J.; Nicoletti, J. W.; San Fillippo, Jr., J.; Jenkins, H. D. B. *J. Am. Chem. Soc.* **1980**, *102*, 1923–1927.

(4) Collman, J. P.; Woo, L. K. *Proc. Natl. Acad. Sci. U.S.A.* **1984**, *81*, 2592–2596.

(5) Collman, J. P.; Garner, J. M.; Woo, L. K. *J. Am. Chem. Soc.* **1989**, *111*, 8141–8148.

(6) We extend the established terminology of conformational analysis to the description of quadruple-bond rotamers. The rotamers are defined by the relative positions of the two meso substituents on the porphyrin macrocycles. The analogy is clear for synperiplanar and antiperiplanar rotamers. The staggered rotamers, synclinal and anticlinal, are defined as 45° rotational isomers of the corresponding periplanar rotamers. The remaining eclipsed rotamer is referred to as simply gauche. Traditionally gauche and synperiplanar are synonymous, but in the analysis of metalloporphyrin dimers we apply the specific designations illustrated in Figure 3.

0002-7863/92/1514-1292$03.00/0

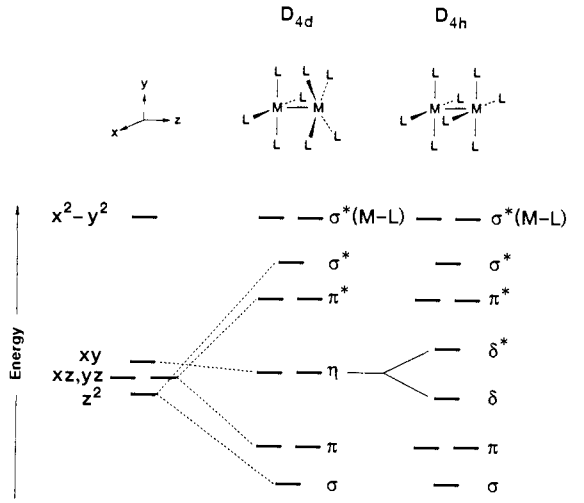

Figure 1. Qualitative molecular orbital diagram for the metal–metal bonds in compounds with M_2L_8 structures.

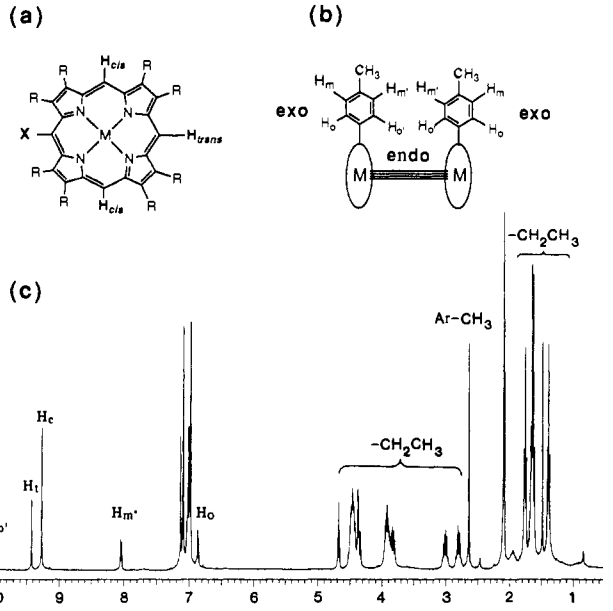

Figure 2. (a) Meso proton regiochemistry in monosubstituted OEP derivatives. (b) Aryl proton regiochemistry in metalloporphyrin dimers. (c) ^{1}H NMR spectrum of $[Mo(TOEP)]_2$ (toluene-d_8, 23 °C).

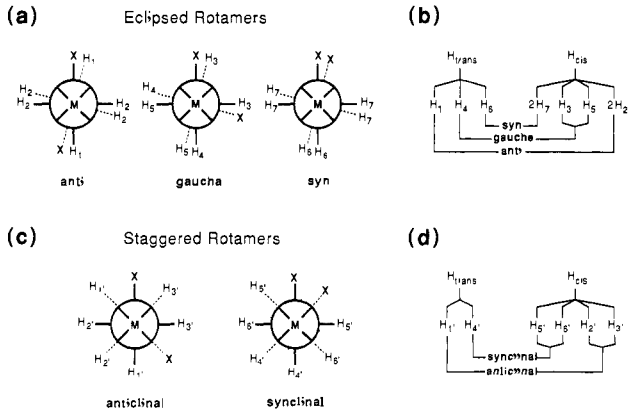

Figure 3. Rotational isomers of about a quadruple metal–metal bond:[6] (a) eclipsed and (c) staggered rotamers. Diagrams of the correlation of rapid rotation (H_{trans} and H_{cis}) to slow rotation in (b) eclipsed, H_1–H_7, and (d) staggered, H_1–H_6, *meso* protons.

An unequivocal determination of ground-state conformation for the unsymmetric molybdenum dimer (OEP)Mo≡Mo(OEP-CHO)[7a,b] was devised by Collman and Woo.[4] At low temperature, the pattern of meso bands of the unsubstituted OEP yield a clear distinction between the observed eclipsed (1:2:1) and alternative staggered (1:1) conformations.[8] This single example established two diagnostic traits of the eclipsed geometry valuable in the analysis of symmetric metalloporphyrin dimers. First, large chemical shift changes with temperature were observed for the meso protons and little, if any, changes were observed for the ethyl group methylene protons. These changes are attributed to through-space deshielding by the meso substituent of the opposing porphyrin and are very dependent on the distance of separation ($\sigma_g \propto r^{-3}$). The greater chemical shift sensitivity of the meso protons relative to the ethyl methylene protons then indicates that the meso substituent is closer to the meso protons in the ground-state conformation. Hence, the ground-state conformation is eclipsed. Second, the single meso proton eclipsed with the meso substituent experiences a pronounced deshielding, thus specifying a regiochemical significance to the individual bands observed in separate rotamers at low temperature.

Scheme I. Relative Strengths of 4d and 5d δ-Bonds

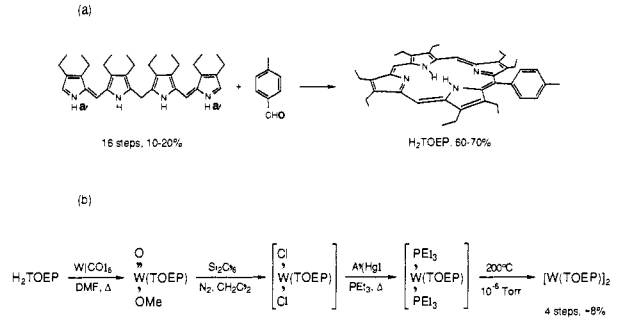

In the current study we compare rotational barriers about the metal–metal bond of mono-*meso*-tolyloctaethylporphyrin dimers, $[M(TOEP)]_2$ (M = Mo, W).[7c] Variable-temperature NMR analysis, discussed in detail below, reveals meso band assignments and chemical shift changes only consistent with eclipsed ground states in both molybdenum and tungsten homologues.

Syntheses. We have recently described the syntheses of tungsten porphyrin dimers by a high-yield four-step procedure.[5] The simplest comparison of isostructural metalloporphyrin dimers would employ the mono-*meso*-formyloctaethylporphyrin (H_2OEP–CHO) used in the previous molybdenum study, but the formyl substituent proved too unstable to allow preparation of the tungsten dimer. Fortunately, a *meso*-4-tolyloctaethylporphyrin (H_2TOEP) prepared via the coupling of *p*-tolualdehyde with octaethyl-1′,8′-dideoxy-*ac*-biladiene dihydrobromide (Scheme Ia)[9] was sufficiently stable to yield $[W(TOEP)]_2$ by the straightforward route outlined in Scheme Ib (a 21-step, ca. 1% total yield).

The preparation of isostructural $[Mo(TOEP)]_2$ by the single-step synthesis with H_2TOEP and $[Mo(CO)_4Cl_2]_2$ and ruthenium and rhenium dimers, $[Ru(TOEP)]_2$ and $[Re^{II}(AHEDMP)]_2$,[7d] by adaptations of procedures developed earlier[10,5] are described in the Experimental Section along with spectroscopic evidence for the formulations given. An attempt to prepare the dicationic form of the rhenium dimer, $\{[Re^{III}(AHEDMP)]_2\}^{2+}$, which would be isoelectronic with the quadruply bonded $[Mo(TOEP)]_2$ and $[W(TOEP)]_2$, was unsuccessful.

(7) Abbreviations: (a) 2,3,7,8,12,13,17,18-octaethylporphyrin (OEP), (b) 5-formyl-2,3,7,8,12,13,17,18-octaethylporphyrin (OEP-CHO), (c) 5-(4-methylphenyl)-2,3,7,8,12,13,17,18-octaethylporphyrin (TOEP), and (d) 5-(4-methoxyphenyl)-2,3,7,8,13,17-hexaethyl-12,18-dimethylporphyrin (AHEDMP) dianions.

(8) Consideration of Figure 3 in which one substituent X group is converted to an H reveals the 1:2:1 ratio of the meso protons of the unsubstituted porphyrin in the eclipsed rotamer (syn:gauche:anti) and a 1:1 ratio in the staggered (synclinal:anticlinal).

(9) (a) Bonnett, R.; Buckley, D. G.; Hamzetash, D. *J. Chem. Soc., Perkin Trans 1* **1981**, 322–325. (b) Johnson, A. W.; Kay, I. T. *J. Chem. Soc. C* **1965**, 1620–1629.

(10) Collman, J. P.; Barnes, C. E.; Swepston, P. N.; Ibers, J. A. *J. Am. Chem. Soc.* **1984**, *106*, 3500–3510.

Table I. ^{1}H NMR Chemical Shifts for Molybdenum- and Tungsten-Porphyrin Dimers

compound	$H_{o'}$	meso	$H_{m'}$	H_m	H_o	CH_2CH_3[a]	$ArCH_3$	CH_2CH_3
$[Mo(TOEP)]_2$[b]	10.06	9.44, 9.29	8.04	7.0	6.84	4.6–3.8	2.64	1.76
						3.00, 2.83		1.64
$[Mo(OEP)]_2$[c]		9.20				4.32, 3.92		1.78
$[Mo(TTP)]_2$[c]	9.63		7.80	7.09	7.09		2.57	
$[W(TOEP)]_2$[b]	9.57	8.80, 8.50	7.91	*d*	*d*	4.22, 3.78	2.59	1.71
						2.95, 2.63		1.64
								1.29
$[W(OEP)]_2$[c]		8.42				4.11, 3.76		1.67

[a] Multiplets. [b] 22 °C, toluene-d_8. [c] 22 °C, benzene-d_6. [d] Overlaps with protio toluene peaks.

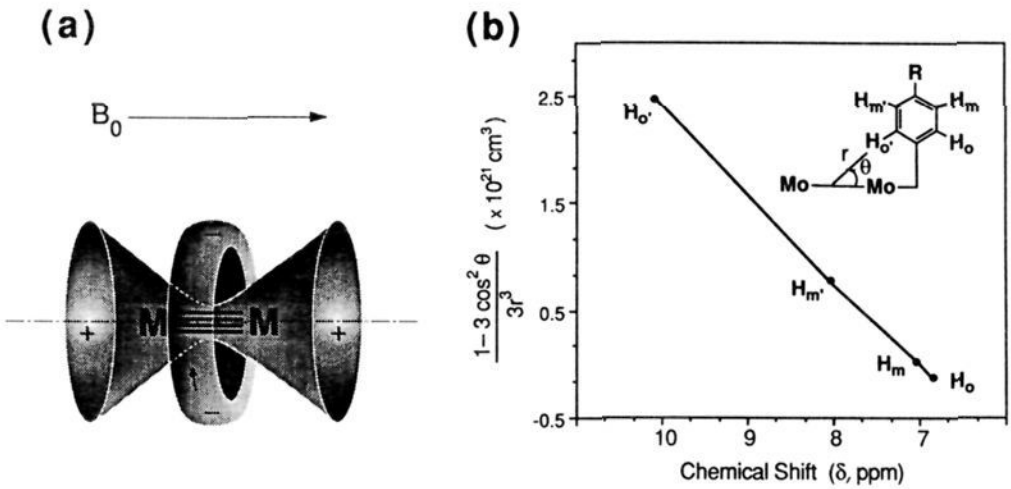

Figure 4. (a) Magnetic anisotropy of the metal–metal bond. (b) Geometric factor of eq 2 vs chemical shift of the aryl protons in $[Mo(TOEP)]_2$.

NMR Analysis of M_2(TOEP)$_2$: Rapid-Rotation Regime. The ^{1}H NMR spectra of $[M(TOEP)]_2$ derivatives in the rapid-rotation regime consist of bands readily assigned to the tolyl group, the meso protons, and the β-ethyl substituents (Figure 2c). A detailed assignment of the spectra of both $[Mo(TOEP)]_2$ (Figure 2) and $[W(TOEP)]_2$ (Table I) requires consideration of the effects of three centers of magnetic anisotropy: the multiple metal–metal bond, the porphyrin macrocycle, and the porphyrin *meso*-tolyl substituent.

Collman and Barnes[10] have shown that the magnetic anisotropy of metal–metal multiple bonds in metalloporphyrin dimers is accurately described by a geometric model based on a point dipole centered between the metals (eq 2).[11a] As with acetylenes, this model defines both a region of deshielding perpendicular to the axis of the multiple bond and conical regions of shielding extending coaxially from the center point (Figure 4a).

$$\sigma_{M\text{-}M} = \frac{(\Delta\chi)(1 - 3\cos^2\theta)}{3r^3(4\pi)} \qquad (2)$$

Both the distance (r) and angle (θ) determine the dipolar shift derived from the metal–metal bond ($\sigma_{M\text{-}M}$). Coordinates from the X-ray structure of $[Mo(TPP)]_2$, reported by Goedken et al.,[12] provide reasonable estimates of r and θ for the tolyl protons of $[Mo(TOEP)]_2$, as shown by the linear dependence of the observed chemical shift on the geometric term of eq 2 (Figure 4b). The *endo*-tolyl protons ($H_{o'}$ and $H_{m'}$), which lie closest to the metal–metal bond (Figure 2b), are more strongly deshielded than the exo protons (H_o and H_m). In particular, the endo-ortho protons ($H_{o'}$) are strongly *deshielded* while the exo-ortho protons (H_o) are *shielded* by the metal–metal bond.[11b]

Deshielding of meso protons by the aromatic porphyrin ring current is well-known. In $[Mo(OEP)]_2$, these protons absorb at 9.20 ppm.[14] As mentioned above, the reduced symmetry of TOEP derivatives yields two distinct meso protons in a 2:1 intensity ratio (see Table I). The chemical shift difference between these meso protons results from both through-bond[15] and through-space contributions of the *meso*-tolyl substituent.

Molecular models and proton NMR experiments[17] indicate that the tolyl ring is positioned roughly perpendicular to the porphyrin

(11) (a) McConnell, H. M. *J. Chem. Phys.* **1957**, *27*, 226–229. (b) The diamagnetic susceptibility ($\Delta\chi$) of the $[M(TOEP)]_2$ quadruple bond is also defined by our analysis: $-16.3\ (\pm 0.8) \times 10^{-33}$ m^3/molecule. This requires that a chemical shift reference ($\sigma_{M\text{-}M} = 0$) be established so that $\sigma_{M\text{-}M}$ can be derived from the experimental values. The tolyl protons of TOEP provide a unique set of chemical shifts which allow this determination. The x intercept of the line connecting the endo- and exo-ortho proton chemical shifts is the ortho reference (7.01 ppm, Figure 4b) and, with $\sigma_{M\text{-}M}$ defined relative to this chemical shift, $\Delta\chi$ can be extracted from the slope of this line. Likewise, a second, and independent, measure of $\Delta\chi$ is produced by the data for the meta protons. The colinearity of these separate sets of data (Figure 4b) provides graphic evidence of their close agreement. Despite the inaccuracy inherent in the assumptions of our structural model, it is clear that $\Delta\chi$ for this quadruple bond is over 1 order of magnitude greater than $\Delta\chi$ for a C≡C bond ($\Delta\chi = -0.34 \times 10^{-33}$ m^3/molecule).[11c] The $\Delta\chi$ of $[Mo(TOEP)]_2$ and that of a previous estimate for $Mo_2(PBu_3)_2(O_2CPh)_2Br_2$ ($\Delta\chi = -10.0\ (\pm 2.5) \times 10^{-33}$ m^3/molecule)[11d,e] support the speculation[11f] that a substantial $\Delta\chi$ is characteristic of quadruple bonds. (c) Harris, R. K. *Nuclear Magnetic Resonance*; Pitman: London, England, 1983; p 193. (d) McGlinchey, M. J.; Burns, R. C.; Hofer, R.; Siden, T.; Hofer, G. *Organometallics* **1986**, *5*, 104–109. (e) McGlinchey, M. J. *Inorg. Chem.* **1980**, *19*, 1392–1394. (f) San Filppo, J. *Inorg. Chem.* **1972**, *11*, 3140–3143.

(12) We construct a model analogous to that reported by Collman and Barnes for the analysis of $[Ru(TPP)]_2$.[10] A metal–metal bond length of 2.239 Å and Cartesian coordinates of an average meso carbon atom (1.81, 6.45 Å), with the origin defined as the midpoint of the metal–metal bond, are those determined for $[Mo(TPP)]_2$.[13] Aryl C–C and C–H bond lengths are assumed to be 1.39 and 1.08 Å.

(13) Yang, C.-H.; Dzugan, S. J.; Goedken, V. L. *J. Chem. Soc., Chem. Commun.* **1986**, 1313–1315.

(14) Collman, J. P.; Barnes, C. E.; Woo, L. K. *Proc. Natl. Acad. Sci. U.S.A.* **1983**, *80*, 7684–7688.

(15) The through-bond effect of a meso substituent on the shielding of OEP-X derivatives is demonstrated by the splitting of the meso protons in monomeric metalloporphyrin derivatives.[16]

(16) (a) Johnson, A. W.; Oldfield, D. *J. Chem. Soc. C* **1966**, 794–798. (b) Bonnett, R.; Stephenson, G. F. *J. Org. Chem.* **1965**, *30*, 2791–2798. (c) Callot, H. J.; Louati, A.; Gross, M. *Tetrahedron Lett.* **1980**, *21*, 3281–3284. (d) Crossley, M. J.; King, L. G.; Pyke, S. M. *Tetrahedron* **1987**, *43*, 4569–4577.

(17) A significant shielding of the methylene protons in the adjacent ethyl group is observed (δ 3.00 and 2.83 vs 4.6–3.8 ppm; Table I), analogous to shifts in {10}paracyclophane: Agarwal, A.; Barnes, J. A.; Fletcher, J. L.; McGlinchey, M. J.; Sayer, B. G. *Can. J. Chem.* **1977**, *55*, 2575–2581.

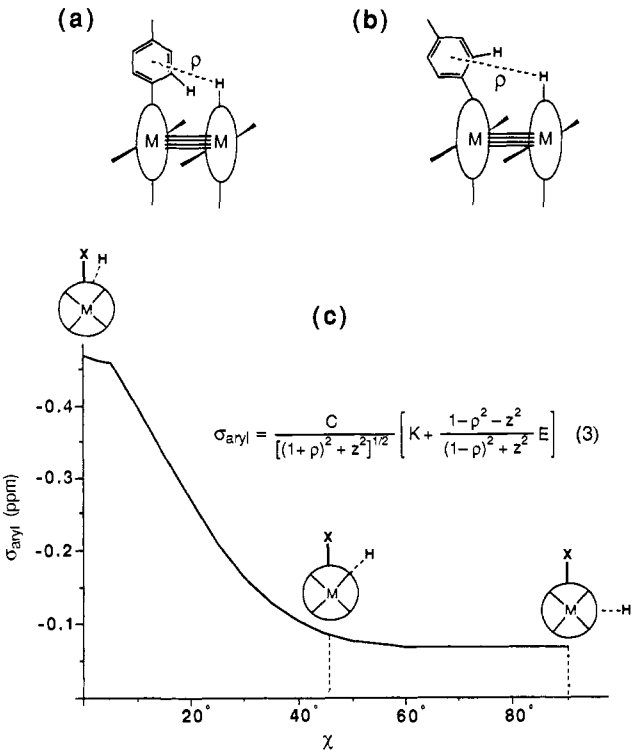

Figure 5. (a) Eclipsed geometry of tolyl and opposing meso proton. (b) "Bending back" distortion of the meso-tolyl substituent. (c) Meso proton shielding due to the ring current of an aryl substituent in a metalloporphyrin dimer as a function angle of rotation about the metal–metal bond (χ).

plane through steric interactions with the adjacent ethyl groups. The dynamic behavior of the ^{1}H NMR ($T < 80$ °C) *is not* complicated by tolyl atropisomerism. A meso proton of the opposing porphyrin which is eclipsed with the meso tolyl group is coplanar with the tolyl protons and is thus deshielded. Due to the relatively accurate description of aromatic ring current (eq 3, Figure 5),[18] we can estimate the magnitude of deshielding expected for a meso proton as a function of rotation about the metal–metal bond through the dihedral angle (χ) defined relative to the tolyl group on the opposite ring.[19] This deshielding is very sensitive to the angle of rotation (Figure 5c) and is negligible when the meso proton is in a staggered position (χ = 45°). As with OEP-CHO dimers, a pronounced deshielding *is only* consistent with a conformation in which the meso proton is eclipsed with the tolyl group. As the chemical shift of a rapid rotation meso band incorporates contributions from more than one rotamer (see Figure 3b,d), the separation of these peaks provides only an indication, a minimum, of the deshielding of a meso proton eclipsed with the tolyl group. In the slow-rotation regime a detailed interpretation of the observed chemical shifts is possible, vide infra.

In all previously studied molybdenum porphyrin dimers, *and in* [*Mo(TOEP)*]$_2$, rapid rotation of porphyrin rings about the metal–metal axis is observed at temperatures above −20 °C.[20] The variable-temperature behavior of [Ru(TOEP)]$_2$, a dimer with a d^{12} electronic configuration and thus a metal–metal bond order of 2 rather than 4, is consistent with rapid porphyrin rotation even at −64 °C.[21] In notable contrast, [W(TOEP)]$_2$ displays rapid rotation only above 50 °C.

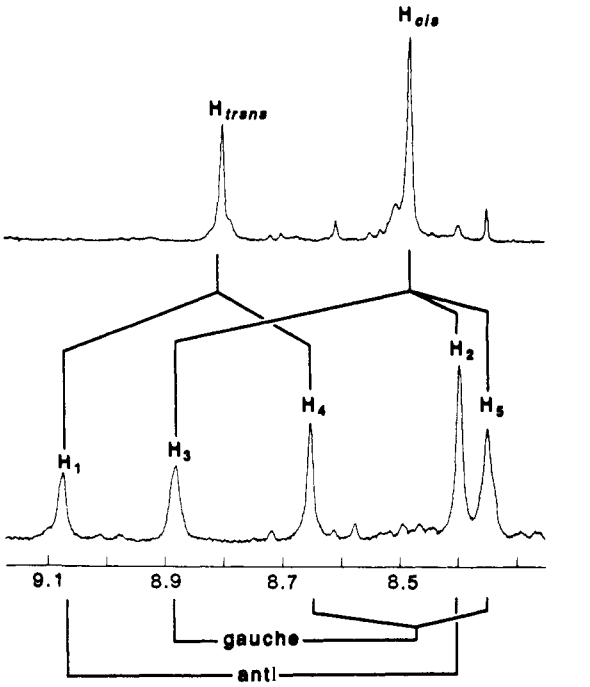

Figure 6. Meso bands (9.2–8.2 ppm) in the proton NMR of [W(TOEP)]$_2$ (toluene-d_8): (a) rapid rotation (51 °C) H_{trans} (8.80, 1.0 H), H_{cis} (8.50, 2.0 H); (b) slow rotation (−48 °C) H_1 (9.07, 1.0 H), H_3 (8.87, 1.63 H), H_4 (8.64, 1.63 H), H_2 (8.39, 2.0 H), H_5 (8.34, 1.63 H).

Slow-Rotation Regime. Four of the rapid-rotation [M(TOEP)]$_2$ bands are simple enough to allow variable-temperature analysis and are unobscured by solvent bands: the two meso bands, H_{trans} and H_{cis}, and the two *endo*-aryl bands, $H_{o'}$ and $H_{m'}$. Despite the similarity of the ^{1}H NMR spectra of [Mo(TOEP)]$_2$ and [W(TOEP)]$_2$ in the fast-rotation regime, differences exist in their low-temperature behavior and rotamer populations. Peak broadening is significant below 50 °C for the tungsten dimer, and *two rotamers* are observed at low temperatures while the meso bands of the molybdenum dimer remain sharp until −25 °C and predominantly *one rotamer* is observed at low temperature.

Five meso bands are resolved in the slow-rotation regime of [W(TOEP)]$_2$ (Figure 6). As the chemical shifts of the rapid rotation peaks, H_{cis} and H_{trans}, are each population-weighted averages, the assignment of the bands which contribute to, for instance, the ν_{trans} (eq 4)[22] specifies the rotamer populations (P_m) which must combine properly to yield the rapid rotation shift of ν_{cis} (eq 5). Attempted assignment of these bands within the staggered conformations (syn- and anticlinal) requires incongruous assignments of chemical shift and rotamer populations.

$$\nu_{trans,ec} = P_a\nu_{H_1} + P_g\nu_{H_4} + P_s\nu_{H_6} \quad (4a)$$

$$\nu_{trans,st} = P_{ac}\nu_{H_{1'}} + P_{sc}\nu_{H_{4'}} \quad (4b)$$

$$\nu_{cis,ec} = (2)P_a\nu_{H_2} + P_g\nu_{H_3} + P_g\nu_{H_5} + (2)P_s\nu_{H_7} \quad (5a)$$

$$\nu_{cis,st} = P_{ac}\nu_{H_{2'}} + P_{ac}\nu_{H_{3'}} + P_{sc}\nu_{H_{5'}} + P_{sc}\nu_{H_{6'}} \quad (5b)$$

If we assume the ground state is eclipsed, the five low-temperature meso peaks require the existence of at least two rotamers, one of which must be gauche. Because there are two downfield eclipsed meso protons in the low-temperature limit (δ 9.06 and 8.87), the anti rotamer must also be present: H_3 of the gauche and H_1 of the anti rotamers are properly oriented (Figure 3a) while

(18) Bovey, F. A. *Nuclear Magnetic Resonance*; Academic Press: New York, 1988; p 108.

(19) We employ the Waugh–Fessenden classical model of ring current magnetic anisotropy as developed by Johnson–Bovey (eq 3).[18] The cylindrical coordinates, ρ and z, are defined with the origin at the center of the tolyl ring. Using the model of [Mo(TOEP)]$_2$ defined above,[12] $z = 0$ and $\rho = 4.28$ Å (Figure 5a) in the perfectly eclipsed conformation (χ = 0°). Rotation about the metal–metal bond increases z and ρ to values of 2.89 and 5.01 Å (χ = 45°), respectively. K and E are the complete elliptic integrals whose modulus k is expressed as $k^2 = (4r)/(1 + \rho^2) + z^2$. $C = ne^2/6\pi M_e c^2 = 8.97$, where n is the number of circulating electrons of charge e and mass M_e and c is the velocity of light. We apply the correction to the Johnson–Bovey calculation suggested by McGlinchey.[17]

(20) Woo, L. K. Ph.D. Dissertation, Stanford University, 1984.

(21) Rapid rotation at −85 °C was also observed for [Re(AHEDMP)]$_2$, a d^{10} dimer with a metal–metal bond order of 3.

(22) Key: ec = eclipsed, st = staggered, a = anti, g = gauche, s = syn, ac = anticlinal, sc = synclinal.

the syn rotamer contains no meso proton eclipsed with the tolyl group. Of these two downfield bands, assignment of the most strongly deshielded peak as H_1 results in a correspondence of rotamer populations consistent with that proposed in Figure 3b. In accord with eq 4a, assignment of the remaining peaks at slow exchange accounts for both meso peaks at fast exchange (T = 51 °C) with $P_a = 0.38$, $P_g = 0.62$, and $P_s = 0.00 \pm 0.02$. Integration of the H_1 and H_4 peaks in the low-temperature limit demonstrates the invariance of these populations throughout the temperature range of these studies. As in $[Mo(OEP\text{-}CHO)]_2$, the syn rotamer is not observed and no more than a slight thermodynamic preference (≤0.2 kcal/mol) for the anti versus the gauche rotamers is found in $[W(TOEP)]_2$.

Further support for the eclipsed ground-state assignments is provided by close agreement of the observed difference in chemical shift of the peaks assigned as H_3 and H_5 (0.47 ppm) and the calculated maximum deshielding expected for the tolyl group eclipsed with a meso proton (0.47 ppm; Figure 5c). These two protons provide an ideal measure of the deshielding as both H_3 and H_5 are H_{cis}, but H_3 is eclipsed with the tolyl group while H_5 is anti to it. Although (OEP)W≡W(TOEP) is not synthetically accessible, the good agreement of calculated and observed through-space deshielding of the meso protons in $[W(TOEP)]_2$ is strong evidence for their eclipsed geometry relative to the tolyl group.

The ^1H NMR of $[Mo(TOEP)]_2$ shows only two meso bands in the slow-rotation regime ($T < -25$ °C) in a 2.1:1.0 ratio (δ 9.29:9.44), consistent with the existence of either a single dominant rotamer at low temperature or a mixture of rotamers with overlapping chemical shifts. The integral ratio, the observed chemical shift changes due to rotation about the metal–metal bond, and analysis of the coalescence line broadening each distinguish between these two possibilities and are all in agreement with a preferred anti rotamer at low temperature.

As only meso protons of the anti (H_1) and gauche (H_3) rotamers are eclipsed with the tolyl substituent, a statistical mixture of all rotamers would yield a 3:1 ratio of shielded to deshielded meso protons. The observed ratio thus excludes an syn population greater than 3% ($P_s < 0.03$). A model of $[Mo(TOEP)]_2$, based on the structure of $[Mo(TPP)]_2$,[13] shows that in *meso*-arylporphyrins steric strain may effect rotamer populations. Even with the doming structure present in $[Mo(TPP)]_2$, the $H_{o'}$ tolyl proton extends across the metal–metal bond to within 0.15 Å of its midpoint. Such an orientation would result in severe tolyl–tolyl rubbing interactions and accounts for the absence of syn rotamers in both $[Mo(TOEP)]_2$ and $[W(TOEP)]_2$.

In a gauche rotamer, one H_{cis} proton is eclipsed with the tolyl group on the opposing porphyrin ring (H_3) and the other (H_5) is anti (Figure 3a). If the two meso bands in the low-temperature regime of $[Mo(TOEP)]_2$ ($\Delta\nu$ = 60 Hz) result from the accidental equivalence of the shielded (H_2, H_4, H_5) and deshielded (H_1, H_3) protons (Figure 3a), then at rapid rotation a statistical population of anti and gauche rotamers ($P_a = 0.33$, $P_g = 0.66$) would yield chemical shifts intermediate and significantly shifted (20 Hz) from those of the low-temperature regime. We observed a very slight change ($\Delta\Delta\nu$ = 3 Hz) of chemical shift between the two meso bands above and below coalescence. Assuming the chemical shift equivalencies described above, this minor shift of high- and low-temperature bands is consistent with no more than a very slight population of the gauche rotamer ($P_g < 0.15$).[23]

Evidence that steric effects influence the relative geometries of $[Mo(TOEP)]_2$ and $[W(TOEP)]_2$ is found in the difference in the chemical shifts of H_1 and H_2 ($\delta_{H_1} - \delta_{H_2}$) in the anti rotamers. This separation largely results from the through-space deshielding of H_1 by the tolyl group on the opposite porphyrin macrocycle. For a given porphyrin geometry, decreasing the metal–metal bond length will increase $\delta_{H_1} - \delta_{H_2}$. Surprisingly, the molybdenum dimer, which is expected to have a shorter metal–metal bond, has a smaller splitting of H_1 and H_2. Either the Mo–Mo bond is longer than the W–W bond or the geometry of the TOEP ligand is distorted so that the eclipsed meso protons are farther from the tolyl ring. If the tolyl group bends away from the metal–metal bond (Figure 5b) to relieve interporphyrin strain, a reduction of the meso proton splitting results. We attribute the weaker splitting of the meso protons of $[Mo(TOEP)]_2$ to such a "bending back" distortion of the tolyl group, induced by porphyrin–porphyrin steric strain, not to a longer metal–metal bond. Evidence that this distortion occurs without weakening of the metal–metal bond is discussed below.

Table II. $\Delta G_{rot}^{\ddagger}$ in $[M(TOEP)]_2$ Determined by Coalescence of Meso H_1 and H_4

metal	T_c (K)	P_a	$\Delta\nu$ (Hz)	$\Delta G^{\ddagger}_{rot}$ (kcal/mol)
W	276 ± 2	0.64	168.8	12.7 ± 0.2
Mo	217 ± 2	0.5 ± 0.5	60 ± 6	10.5 ± 0.5

δ-Bond Rotational Barriers: Coalescence Point Analysis. Of the four meso proton NMR bands of $[W(TOEP)]_2$ which may be analyzed by variable-temperature techniques, the simple coalescence point formula, adapted for the treatment of unequally populated doublets,[25] can only be applied to the meso H_1 and H_4 protons. Using the separation of the meso H_1 and H_4 peaks from the slow-exchange limit ($\Delta\nu_{H_1\text{-}H_4}$ = 168.8 Hz), the relative population of the anti and gauche isomers determined from eq 3, and a coalescence temperature (T_c) of 3 °C, a rotational barrier of 12.7 ± 0.2 kcal/mol is calculated for $[W(TOEP)]_2$ (Table II).

The same calculation for $[Mo(TOEP)]_2$ requires an approximation for $\Delta\nu$ and P_a. The frequency difference between H_1 and H_4 ($\Delta\nu_{H_1\text{-}H_4}$) may be estimated by the observed difference between H_1 and H_2 ($\Delta\nu_{H_1\text{-}H_2}$). Due to their identical positions relative to the opposing tolyl group, the angular dependence of σ_{tolyl} (Figure 5) predicts chemical shift equivalence for H_2 and H_4. As a test of this approximation, the same assumption for $[Mo(OEP\text{-}CHO)]_2$ (a dimer with H_1, H_2, and H_4 resolved at low temperature) yields only a 10% error in $\Delta\nu$. As the anisotropy of the formyl group in $[Mo(OEP\text{-}CHO)]_2$ is stronger than that of the tolyl group in $[Mo(TOEP)]_2$,[28] this provides a conservative error limit on the above approximation (Table II).

Next, P_a must also be estimated. We employ the adaptation of the coalescence point formula to analyze an unequally populated doublet.[25] It is important to note that the population assignment contributes little to the magnitude of $\Delta G^{\ddagger}_{rot}$ (±0.14 kcal/mol for $1 \geq P_a \geq 0$). Although the bandshape analysis described below yields an assignment of $P_a = 0.85$, a failsafe estimate of $P_a = 0.5 \pm 0.5$ is used for the coalescence point calculation listed in Table II. Thus, for any value of P_a, a barrier of 10.5 ± 0.5 kcal/mol is obtained which closely agrees with barriers previously measured for the series of molybdenum–porphyrin dimers (10.3 ± 0.5 kcal/mol).[4]

Complete Bandshape Analysis. The meso, $H_{o'}$, and $H_{m'}$ protons of $[W(TOEP)]_2$ provide four separate spin systems that may be analyzed through complete bandshape (CBS) analysis. As each spin system is characterized by a separate set of spectral parameters, a multiple verification of rate results from the best fit of all four simulations at a given rate. The calculated and experimental spectra are compared in Figure 7. The barrier for interconversion of the anti and gauche rotamers ($\Delta G^{\ddagger}_{rot}$ = 12.9 ± 0.1 kcal/mol), determined from an Eyring plot of these best-fit rates versus $1/T$ (Figure 8) is in excellent agreement with the coalescence point analysis. The very low value of $\Delta S^{\ddagger}_{rot}$ renders this barrier temperature independent, within experimental error: $\Delta G^{\ddagger}_{rot} = \Delta H^{\ddagger}_{rot}$.

(23) A useful approximation[24] is that the change of chemical shift $\Delta\Delta\nu = P_g(\Delta\nu)$.

(24) Anet, F. A. L.; Basus, V. J. *J. Magn. Reson.* **1978**, *32*, 339–343.

(25) We have used the method of Shanan-Atidi and Bar-Eli[26] which has been conveniently tabulated by Sandström.[27a]

(26) Shanan-Atidi, H.; Bar-Eli, K. H. *J. Chem. Phys.* **1970**, *74*, 961–963.

(27) (a) Sandström, J. *Dynamic NMR Spectroscopy*; Academic: New York, 1982; p 82. (b) Berg, U.; Sandström, J. *Adv. Phys. Org. Chem.* **1989**, *25*, 1–97.

(28) $\delta_{H_1} - \delta_{H_2}$ = 0.46 in $[Mo(OEP\text{-}CHO)]_2$ vs 0.15 ppm in $[Mo(TOEP)]_2$.

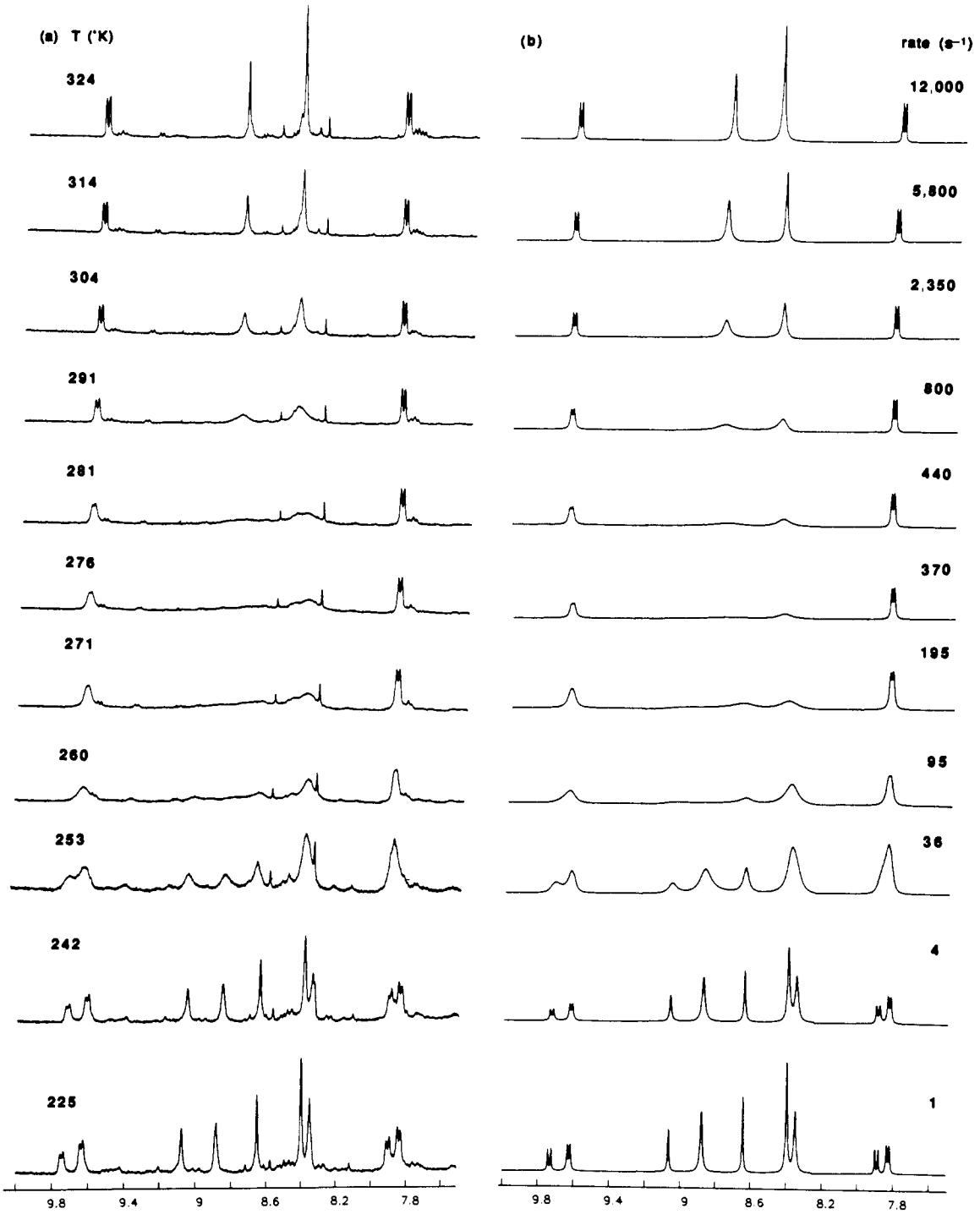

Figure 7. Variable-temperature ^1H NMR spectra of $[W(TOEP)]_2$: (a) experimental and (b) calculated.

The variable-temperature rate data from the CBS analysis of the molybdenum dimer meso protons is also shown in Figure 8. Again, the barrier agrees well with that determined by the coalescence point analysis: $\Delta G^*_{rot} = 10.8 \pm 0.1$ kcal/mol. Comparison of the fast- and slow-rotation chemical shifts of either meso band shows very little change (3 Hz), but significant broadening occurs at coalesence. This pair of observations is diagnostic of an exchange between sites with very different populations ($P_a \gg P_g$) and a large difference in chemical shift.[24] Using the same approximation of $\Delta\nu$ as in the coalescence point calculation above yields a better estimate of $P_a = 0.85 \pm 0.10$.

Discussion

The description of quadruple bonds between metal atoms has led to speculation and debate on the strength of these bonds and, in particular, the strength of the δ-bond. A number of years ago we reported studies demonstrating rotational barriers about the metal–metal quadruple bond of molybdenum–porphyrin dimers[4] were of appropriate magnitude[29] to observe and analyze through variable-temperature, DNMR,[30] analysis. As a measure of δ-bond strengths, these barriers (10.3 ± 0.5 kcal/mol) agree with the spectroscopic analysis of Trogler and Gray which placed an upper limit of 20 kcal/mol for δ-bonds.[31] Moreover, the rotational barrier measurement is free from a variety of assumptions that have complicated a direct correlation of other spectroscopic data

(29) Early, inflated estimates of δ-bond strengths[1a,b] led some scientists to conclude that NMR would be an inappropriate tool to measure these bond strengths. See: Chisholm, M. H. *Reactivity of Metal-Metal Bonds*; Chisholm, M. H., Ed.: American Chemical Society: Washington, DC, 1981; pp 17–39.

(30) Binsch, G.; Kessler, H. *Angew. Chem., Int. Ed. Engl.* **1980**, *19*, 411–428; *Angew. Chem.* **1980**, *92*, 331.

(31) Trogler, W. C.; Gray, H. B. *Acc. Chem. Res.* **1978**, *11*, 232–239.

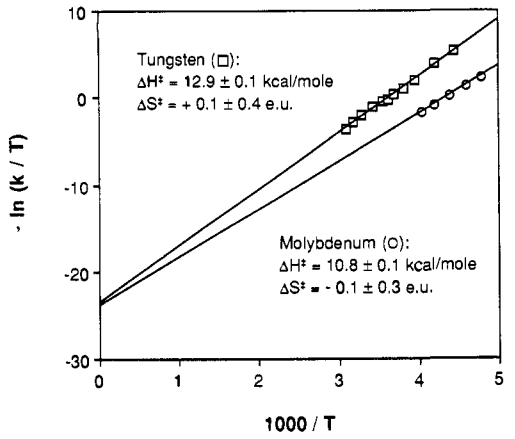

Figure 8. Eyring plot for rotation about the metal–metal bond axis in $[M(TOEP)]_2$.

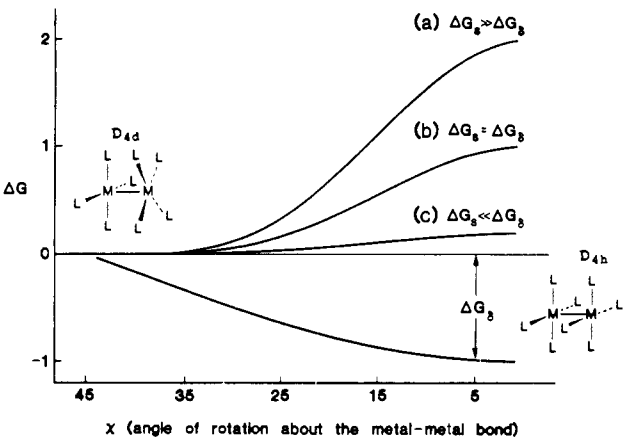

Figure 9. Electronic stabilization and steric destabilization as a function of rotation about the metal–metal bond: $\chi = 0°$ (eclipsed), $\chi = 45°$ (staggered); ΔG_s = ligand–ligand steric repulsion, ΔG_δ = electronic stabilization of the δ-bond.

to δ-bond strength. Such complications have led to opposing conclusions as to the relative strengths of δ-bonds in $[M_2]^{4+}$ dimers of molybdenum, a 4d metal, and tungsten, a 5d metal.

Despite synthetic difficulties in preparing compounds with tungsten–tungsten quadruple bonds, a number of isostructural molybdenum and tungsten dimers exist: $M_2(CH_3)_8^{4-}$,[32] $M_2X_4(PR_3)_4$,[33] $M_2(mhp)_4$,[34] and $M_2(O_2CR)_4$[35] (M = Mo, W). In all cases, structural characterization has demonstrated that *the W–W bond length is greater than the Mo–Mo distance* by ~0.1 Å.[36] Because the two metal d_{xy} orbitals are not directed at each other along the metal–metal axis, δ-overlap will be more sensitive to the metal–metal distance than the metal–metal π- and σ-overlap. One contention has been the longer metal–metal bonds in tungsten analogues will result in a weaker δ-bond based upon overlap. Gas-phase photoelectron measurements with volatile $[M_2]^{4+}$ dimers[37] and certain comparisons of the intensities and energies of assigned $\delta \rightarrow \delta^*$ electronic transitions within a series of related quadruple bonds[32b,33a,38] support stronger molybdenum versus tungsten δ-bonds. Recent work by Hopkins, Gray, and Miskowski,[33c] however, indicates that other factors independent of δ-bond strengths strongly influence the intensities and energies of these electronic transitions. The simple comparison of $\delta \rightarrow \delta^*$ energies with M–M bond lengths assumes these factors are the same for different metals, whereas detailed analyses[33c] and calculations[2] indicate this assumption is not valid, especially for comparisons of 4d versus 5d metals. Manning and Trogler[34b] have proposed that increased radial extension of 5d orbitals compensates for longer metal–metal bond lengths and interpret the $\delta \rightarrow \delta^*$ electronic transitions of a series of molybdenum and tungsten dimers in support of a stronger δ-bond for the isostructural tungsten dimers. We conclude that the lack of an unambiguous measure of δ-bond strength to correlate with structural data clouds the extent to which the relative δ-bond strengths contribute to longer metal–metal distances for the tungsten homologues.

We have measured rotational barriers (ΔG^*_{rot}) for $[Mo(TOEP)]_2$ and $[W(TOEP)]_2$ of 10.8 and 12.9 kcal/mol, respectively, and demonstrated that both dimers possess an eclipsed ground state. As the δ-bond requires d_{xy}–d_{xy} overlap across a metal–metal bond (Figure 1), the strength of the δ-bond is dependent on the angle of rotation about this bond axis (Figure 9), conveniently expressed as the dihedral angle, χ, between ligands on adjacent metal centers (L—M≡M—L). When $\chi = 45°$, the conformation is "staggered" (D_{4d}), and, due to the out-of-phase orientation of the two d_{xy} orbitals, the δ-bond is at a rigorous zero-valued minimum (η in Figure 1 and $\Delta G_\delta = 0$ in Figure 9). When $\chi = 0°$, the conformation is "eclipsed" (D_{4h}) and the δ-bond is at maximum strength ($\Delta G_\delta = -1$, Figure 9). We assume that ligand–ligand steric interactions are also at a minimum when $\chi = 45°$ and at a maximum when $\chi = 0°$, but because they are repulsive ($\Delta G_s > 0$, Figure 9) they weaken the metal–metal bond.

Three experimentally distinct ground states thus derive from limiting combinations of ΔG_δ, which strengthens the metal–metal bond, and ΔG_s, which weakens it (Figure 9): (a) $\Delta G_s \gg \Delta G_\delta$ yields a staggered ground state, (b) $\Delta G_s \approx \Delta G_\delta$ yields a ground state with no conformational preference,[39] and (c) $\Delta G_s \ll \Delta G_\delta$ yields an eclipsed ground state. Our results are consistent with the latter, confirming the dominant relative strength of δ-bonds in both of these metalloporphyrin dimers. A conclusion on the relative δ-bond strengths of $[Mo(TOEP)]_2$ and $[W(TOEP)]_2$, however, requires us to address the more subtle issue of the relative magnitude of weak steric interactions: Is *the difference* in the rotational barriers of $[Mo(TOEP)]_2$ and $[W(TOEP)]_2$ (2.1 kcal/mol) due to the difference in δ-bond strengths or the difference in weak steric interactions?

Structural features from the two crystallographically characterized metalloporphyrin dimers, $[Mo(TPP)]_2$[13] and $[Ru(OEP)]_2$,[10] provide a reasonable model for considering the porphyrin–porphyrin steric interactions in $[M(TOEP)]_2$. As expected, the quadruple metal–metal bond of the molybdenum dimer is shorter than the formal double bond of the ruthenium dimer (2.239 vs 2.408 Å, $\Delta r_{M-M} = 0.17$ Å). However, compensating differences in the "doming" structure, the distance that each metal is displaced from the plane of the four pyrrole nitrogens (0.46 Å for Mo vs 0.30 Å for Ru), results in average macrocycle plane to plane

(32) (a) Cotton, F. A.; Troup, J. M.; Webb, T. R.; Williamson, D. H.; Wilkinson, G. *J. Am. Chem. Soc.* **1974**, *96*, 3824–3828. (b) Collins, D. M.; Cotton, F. A.; Koch, S. A.; Millar, M.; Murillo, M. *Inorg. Chem.* **1978**, *17*, 2017–2020.

(33) (a) Cotton, F. A.; Extine, M. W.; Felthouse, T. R.; Kolthammer, B. W. S.; Lay, D. G. *J. Am. Chem. Soc.* **1981**, *103*, 4040–4045. (b) Cotton, F. A.; Felthouse, T. R.; Lay, D. G. *Ibid.* **1980**, *102*, 1431–1433. (c) Hopkins, M. D.; Schaefer, W. P.; Bronikowski, M. J.; Woodruff, W. H.; Miskowski, V. M.; Dallinger, R. F.; Gray, H. B. *Ibid* **1987**, *109*, 408–416.

(34) (a) Cotton, F. A.; Fanwick, P. E.; Niswander, R. H.; Sekutowski, J. C. *J. Am. Chem. Soc.* **1978**, *100*, 4725–4732. (b) Manning, M. C.; Trogler, W. C. *J. Am. Chem. Soc.* **1983**, *105*, 5311–5320.

(35) (a) Cotton, F. A.; Mester, Z. C.; Webb, T. R. *Acta Crystallogr.* **1974**, *B30*, 2768–2770; (b) Chisholm, M. H.; Chiu, H. T.; Huffman, J. C. *Polyhedron* **1984**, *3*, 759–760.

(36) The difference between molybdenum and tungsten bond lengths is greater for complexes containing quadruple bonds than in the metals (0.01 Å) or other M–M-bonded complexes.[32b]

(37) (a) Bursten, B. E.; Cotton, F. A.; Cowley, A. H.; Hanson, B. E.; Lattman, M.; Stanley, G. G. *J. Am. Chem. Soc.* **1979**, *101*, 6244–6249. (b) Garner, C. D.; Hillier, I. H.; Knight, M. J.; MacDowell, A. A.; Walton, I. B.; Guest, M. F. *J. Chem. Soc., Faraday Trans. II* **1980**, *76*, 885–894. (c) Cotton, F. A.; Hubbard, J. L.; Lichtenberger, D. L.; Shim, I. *J. Am. Chem. Soc.* **1982**, *104*, 679–686.

(38) (a) Sattelberger, A. P.; Fackler, J. P. *J. Am. Chem. Soc.* **1977**, *99*, 1258–1259. (b) Cotton, F. A.; Kock, S.; Mertis, K.; Millar, M.; Wilkinson, G. *Ibid.* **1977**, *99*, 4989–4992. (c) Clark, R. J. H.; D'Urso, N. R. *Ibid.* **1978**, *100*, 3088–3091. (d) Bohmer, W. H.; Madeja, K.; Kurras, E.; Rosenthal, U. *Z. Chem.* **1978**, *18*, 453–454. (e) Fanwick, P. E.; Bursten, B. E.; Kaufmann, G. B. *Inorg. Chem.* **1985**, *24*, 1165–1169.

(39) Smith and Goddard propose that $[Re_2Cl_8]^{2-}$ falls into this category with a 6 kcal/mol δ-bond and 3 kcal/mol of offsetting steric repulsion, yielding a net 3 kcal/mol rotational barrier.[3a]

distances that are very similar (3.21 vs 3.26 Å, $\Delta r_{P-P} = 0.05$ Å).[40] As discussed above,[32-36] the difference in $[Mo_2]^{4+}$ and $[W_2]^{4+}$ quadruple bond lengths should be less than 0.17 Å, so the porphyrin–porphyrin plane-to-plane separation in $[Mo(TOEP)]_2$ and $[W(TOEP)]_2$ is expected to be insensitive to the metal–metal bond length.

In metalloporphyrin dimers with "linear substituents" at the meso position the separation of the N_4 planes represents the closest nonbonding contact between the porphyrin macrocycles. Alternatively, in dimers containing a *meso*-aryl substituent, the endo protons of the aryl group project across the metal–metal bond and are the closest porphyrin–porphyrin contacts. Thus, despite a shorter metal–metal bond, the N_4–N_4 separation in $[Mo(TPP)]_2$ is longer than in $[Ru(OEP)]_2$ (3.155 vs 3.008 Å, $\Delta r_{N-N} = 0.15$ Å). We attribute this difference to the effect of the *meso*-aryl substituents. In the eclipsed conformation, significant rubbing interactions between aryl groups cannot be avoided in a tetraarylporphyrin. As a result, the porphyrin cores of $[Mo(TPP)]_2$ are rotated 18° out of the eclipsed geometry.[41] Neither $[W(TOEP)]_2$ nor $[Mo(TOEP)]_2$ populates the syn rotamer, so no analogous steric effect can be attributed to the same tolyl–tolyl repulsion in these dimers.

Variable-temperature NMR analyses of both $[Ru(TOEP)]_2$ and $[Re(AHEDMP)]_2$ are consistent with rapid rotation about the metal–metal bond, even at −64 °C.[43] The difference in interporphyrin plane to plane separation of $[Ru(OEP)]_2$ (3.26 Å) and $[Mo(TPP)]_2$ (3.21 Å) is small, and it is likely that the same difference of separation in ruthenium- and molybdenum–TOEP derivatives is equally insignificant. The molecular orbital description of the bonding in metal dimers (Figure 1) predicts a net bond order of 2 for $[Ru(TOEP)]_2$ ($\sigma^2\pi^4\delta^2\delta^{*2}\pi^{*2}$) and 3 for $[Re(AHEDMP)]_2$ ($\sigma^2\pi^4\delta^2\delta^{*2}$). Neither of these dimers possess a δ-bond or a detectable rotational barrier.[43] This places an important limit on steric effects in $[Mo(TOEP)]_2$. For instance, an observed $\Delta G^{\ddagger}_{rot}$ of 10 kcal/mol could result from a ΔG_s of 10 kcal/mol coincident with a ΔG_δ of 20 kcal/mol. In such a case loss of the δ-bond would reveal a rotational barrier derived from the steric effects. In the dimers $[M(TOEP)]_2$ this is not the case. If no basis for an electronic barrier exists, then no rotational barrier, detectable by NMR, is observed ($\Delta G_s < 7.6$ kcal/mol).

Rotational barriers in metallocenes, which have very similar plane to plane separations (~3.3 Å), do not exceed 5.0 kcal/mol for monosubstituted derivatives.[44b] Barriers of this magnitude could account for *the difference* observed in electronic barriers of the molybdenum and tungsten dimers. A more direct and sensitive probe of the steric effect of a *meso*-aryl substituent on the δ-bond strength is derived from the comparison of previously determined barriers for $[Mo(OEP\text{-}X)]_2$ with X = formyl, isocyanate, and NH_2 (10.3 ± 0.5), with the barrier which we observe for X = tolyl (10.8 ± 0.1).

As discussed above, when an *meso*-aryl substituent is in a conformation perpendicular to the porphyrin plane, the endo protons project across the metal–metal bond near to its midpoint. The adjacent β-pyrrolic ethyl groups in TOEP lock the tolyl group in such a conformation, as evidenced by the ring current shielding of their methylene protons.[17] In this geometry, only a "bending back" distortion of the tolyl ring (Figure 5b) or a lengthening of the metal–metal bond can relieve the steric repulsion between the tolyl group and the opposing porphyrin macrocycle. We have explained the reduced magnitude of deshielding experienced by the meso protons of the molybdenum vs tungsten dimer as the result of the difference in the bending back of their tolyl groups. This distortion is consistent with a shorter metal–metal bond length in the molybdenum dimer and apparently occurs *without significant sacrifice of free energy* as the $[Mo(TOEP)]_2$ barrier is within experimental error of such linear substituents as isocyanate, which do not project across the metal–metal bond axis. In fact, the TOEP dimer appears to have a slightly stronger δ-bond. The insensitivity of the rotational barrier to increased porphyrin–porphyrin strain demonstrates that the steric component of the barrier is less than the difference between the measured barriers of these related OEP derivatives ($\Delta G_s < 0.5$ kcal/mol). Because the steric component of the tungsten barrier must be less than that of the molybdenum barrier, the difference between these steric components must also be less than 0.5 kcal/mol. This conclusion is critical to our comparison of rotational barriers in molybdenum and tungsten dimers. The measured difference (2.1 kcal/mol) cannot be attributed to the difference in porphyrin–porphyrin steric repulsion.

Previous studies have noted the sensitivity of energies and intensities of $\delta \rightarrow \delta^*$ electronic transitions to the nature of ligands stabilizing the $[M{\equiv}M]^{n+}$ unit. Even halide substitution in the series $Mo_2X_4(PMe_3)_4$, where X = Cl, Br, and I, causes dramatic changes in these electronic parameters though the structural parameters are quite similar.[45] Researchers have attributed these changes to differences in metal–metal δ,δ* mixing with ligand π-orbitals which, in turn, may indicate a strong effect of different ligand sets on δ-bond strengths. The d_{xy} orbital of each metal in the $[M{\equiv}M]^{n+}$ unit has the opportunity to form both a weak δ-bond with its dimetal counterpart and π-bonds with a ligand orbital set. The extent to which the metal forms π-bonds with ligand orbitals should intuitively influence the metal–metal δ-bond strength and depend on the metal and ligand set. In our study, the use of isostructural dimers with the same porphyrin (TOEP) should simplify the extrapolation that the measured rotational barriers are true δ-bond strengths in this system. But the comparison of $[Mo(TOEP)]_2$ and $[W(TOEP)]_2$ rotational barriers, like any other comparison of 4d and 5d δ-bond strengths using electronic, theoretical, or photoelectronic measurements, must still contend with the possibility that the metals interact differently with ligand orbitals even though all $[M{\equiv}M]^{n+}$ units experience the same ligand environment. This latter point illuminates a tremendous advantage in studying the relative δ-bond strengths in the metalloporphyrin system. That is, the metal d_{xy} orbitals are virtually innocent of any porphyrin orbital mixing as no symmetry-allowed interaction can occur between these orbitals and porphyrin π-orbitals. Hence, the metal–metal δ-bonding orbitals should be virtually 100% metal in character.[46] For this reason, we are confident that the differences we measure for the molybdenum and tungsten δ-bond strengths are not the result of differences in metal δ,δ* mixing with porphyrin orbitals.

Conclusions

The rotational barriers reported for $[Mo(TOEP)]_2$ and $[W(TOEP)]_2$, $\Delta G^{\ddagger}_{rot}$ = 10.8 and 12.9 kcal/mol, respectively, establish a more than 2 kcal/mol stronger barrier for the tungsten dimer. The magnitude of this *electronic barrier* in $[W(TOEP)]_2$ is remarkable, although in reasonable agreement with the intrinsic δ-bond strength proposed by Hopkins, Gray, and Miskowski (~10

(40) Recent vibrational analyses of both $[Ru(OEP)]_2$ and $[Mo(OEP)]_2$ show no evidence of π-orbital overlap,[40a,b] although the broadening and blue shift of the Soret band in $[Ru(OEP)]_2$ has been attributed to excitonic interactions of the porphyrin macrocycles.[10] (a) Tait, C. D.; Garner, J. M.; Collman, J. P.; Sattelberger, A. P.; Woodruff, W. H. *J. Am. Chem. Soc.* **1989**, *111*, 7806–7811. (b) Tait, C. D.; Garner, J. M.; Collman, J. P.; Sattelberger, A. P.; Woodruff, W. H. *J. Am. Chem. Soc.* **1989**, *111*, 9072–9077.

(41) The cos (2χ) dependence of the metal–metal bond length on the torsional angle χ demonstrated by Cotton for a series of bridged $Mo_2Cl_4L_4$ dimers suggests that a rotation of 18° (40% of the rotation towards a staggered conformation) would result in a loss of only 20% of the δ-bond strength.[42]

(42) Cambell, F. L., III; Cotton, F. A.; Powell, G. L. *Inorg. Chem.* **1984**, *23*, 4222–4226.

(43) The rotational barrier limit detectable by NMR[27b] can be lowered by the large isotropic shifts observed in paramagnetic complexes.[44a] $[Ru(TOEP)]_2$ is paramagnetic, and the resulting increased separation of the meso bands (H_{cis} and H_{trans}), $\Delta\delta$ = 10 ppm at −64 °C, allows a reduced lower limit on the rotational barrier ($\Delta G_{rot} < 7.6$ kcal/mol).

(44) (a) Moore, R. M., Jr.; Streitwieser, A., Jr.; Wang, H. K. *Organometallics* **1986**, *5*, 1418–1421. (b) Luke, W. D.; Streitwieser, A., Jr. *J. Am. Chem. Soc.* **1981**, *103*, 3241–3243.

(45) These factors include the nature and relative energies of δ,δ* ground and excited states, as well as the extent of δ,δ* orbital mixing with ligand orbitals: (a) Hopkins, M. D.; Gray, H. B.; Miskowski, V. M. *Polyhedron* **1987**, *6*, 705–714. (b) Reference 33c.

(46) MO calculations for other quadruply bonded systems would predict δ,δ* orbitals with ca. 60–85% metal character (see ref 3a and references therein).

kcal/mol).[45a] As the differences in ligand–ligand and metal–ligand interactions are arguably insignificant, we conclude that in isostructural metalloporphyrin dimers the ditungsten intrinsic δ-bond strength is 2.1 ± 0.5 kcal/mol greater than the dimolybdenum δ-bond strength.

Our analysis concurs with the trend of longer quadruple bond lengths in unbridged tungsten (5d) vs molybdenum (4d) dimers, but our conclusion, based on quadruple-bond rotational barriers, stands in contrast to that arrived at by the analysis of $\delta \rightarrow \delta^*$ electronic transitions for $[M(CH_3)_4]_2^{2-}$ and $[MX_2(PR_3)_2]_2$ (M = Mo, W).[32b,37] A stronger tungsten δ-bond is consistent with the trend of increasing bond strengths to metals as one descends a column of transition elements in the periodic table. Our results and the M–X bond strengths of $Cp(CO)_3M-M(CO)_3Cp$,[47] $Cp(CO)_3M-H$,[48] and $[Cp(CO)_2LM{=}CH_2]^+$ (M = Mo, W)[49] demonstrate that greater radial extension of 5d orbitals leads not only to longer and stronger σ- and π-bonds but also to stronger δ-bonds.

Correlations between length and strength in δ-bonds must be made with caution!

Experimental Section

Solvents and Reagents. Toluene and benzene solvents for drybox use were distilled from their purple sodium benzophenone ketyl solutions under a dry nitrogen atmosphere. These solvents were subsequently degassed in the drybox by bubbling box atmosphere gas through the solutions for 20–30 min. Deuterated solvents ($C_6D_5CD_3$, C_6D_6) were dried similarly and then degassed on a vacuum line (10^{-5} Torr) with three successive freeze–pump–thaw cycles. DMF was stirred over $MgSO_4$ (24 h), filtered, vacuum distilled (76 °C, 39 Torr), and stored over activated (200 °C, 0.01 Torr) sieves (Linde, 4X). PEt_3 (Alfa) was stirred over Al(Hg) for 24 h prior to use under a nitrogen atmosphere. Argon for Schlenkware reactions was dried by passage over activated sieves. Flash chromatographic silica (EM Science, Kieselgel 60H), gravity alumina (Fischer, Neutral, 80–200 mesh), and Celite for drybox use were predried at 300 °C overnight, then further dried and degassed under vacuum (300 °C, 0.01 Torr) for 24 h, and stored in the drybox. The Si_2Cl_6 (Aldrich) and $W(CO)_6$ (Pressure Chemical) reagents were used without further purification. Al(Hg) was prepared by a literature procedure.[50]

Instruments and Measurements. All manipulations of air-sensitive compounds were performed in a drybox, in Schlenkware, or on a vacuum line. The pyrolysis tube used in the solid-state syntheses below was equipped with a high-vacuum E. J. Young stopcock and an O-ring vacuum adapter. The drybox was a Vacuum Atmospheres HE-553-2 Dri-Lab with a MO-40-1H Dri-Train under nitrogen atmosphere. Oxygen levels were monitored with a AO 316-C trace oxygen analyzer and were maintained ≤1 ppm.

^1H NMR spectra were recorded with a 300-MHz Nicolet NMC-300 instrument with a FT 1280 disk data system or an Varian XL-400. Chemical shifts are reported in units of δ (downfield from tetramethylsilane) but were measured relative to residual ^1H resonances in deuterated solvents: $CHCl_3$ (7.25), C_6D_5H (7.15), and $C_6D_6CD_2H$ (2.09). Variable-temperature experiments were calibrated by the frequency difference method[51] with neat methanol, under vacuum, in a sealed NMR tube. Lineshape analyses were performed using the program DNMR5 adapted for operation on a personal computer.[52]

A Cary 219 spectrophotometer was used to record UV–visible spectra (300–825 nm). LSI mass spectra of air-stable compounds utilized a tetraglyme matrix. FAB mass spectroscopy was performed at the California–Berkeley chemistry department mass spectroscopy facility using an air-sensitive technique and a sulfolane matrix. The calculated isotope intensities matched well with the observed molecular or fragment ion isotope clusters for all compounds analyzed.

5-(4-Methoxyphenyl)-2,3,7,8,13,17-hexaethyl-12,18-dimethylporphyrin, H_2AHEDiMP (1). 1′,8′-Dideoxy-1,2,4,5,7,8-hexaethyl-3,6-dimethyl-*ac*-biladiene dihydrobromide[53] (100 mg, 0.151 mmol) was suspended in methanol (25 mL) containing 4-methoxybenzaldehyde (239 mg, 1.76 mmol) and four drops of 48% aqueous HBr; the mixture was then boiled for 48 h. The solution was cooled and treated with $NaHCO_3$ (0.2 g) dissolved in water (25 mL). After the mixture was stirred for 15 min, the purple precipitate was collected by vacuum filtration, washed with water (50 mL), redissolved in CH_2Cl_2, filtered, and then evaporated. The purple residue was redissolved in the minimum amount of toluene and flash chromatographed (SiO_2, 4 × 10 cm). The major dark red band eluted with the same solvent and was crystallized from CH_2Cl_2/CH_3OH as purple needles (61 mg, 66%). ^1H NMR ($CDCl_3$): H_{meso} 10.14 (s, 2 H), 9.88 (s, 1 H); aryl H_o 8.09 (d, 8.5 Hz, 2 H), H_m 7.20 (d, 9.4 Hz, 2 H); CH_2CH_3 4.2–3.9 (m, 8 H), 2.82 (q, 7.4 Hz, 4 H); OCH_3 3.62 (s, 3 H); CH_2CH_3 2.0–1.75 (m, 12 H), 1.15 (t, 7.4 Hz, 6 H); CH_3 1.52 (s, 6 H); NH −3.0 (d, 2 H). LSIMS (tetraglyme): m/e = 613 (cluster, M^+). UV–vis (CH_2Cl_2; λ_{max}, nm): 406, 504, 537, 570, 622.

5-(4-Methylphenyl)-2,3,7,8,12,13,17,18-octaethylporphyrin, H_2TOEP (2). 3,4-Diethyl-2-formylpyrrole[53] (605 mg, 4.00 mmol) and 3,3′,4,4′-tetraethyldipyrromethane-5,5′-dicarboxylic acid[54] (689 mg, 2.00 mmol) were dissolved in hot methanol (25 mL) and then 48% aqueous HBr (3 mL) was added. The solution was immediately turned dark red, and a gas evolved. The solution was allowed to cool to room temperature during which time lustrous green crystals formed. The mixture was cooled to −20 °C overnight, and then the solid was isolated by vacuum filtration. The green crystals of 1′,8′-dideoxy-1,2,3,4,5,6,7,8-octaethyl-*ac*-biladiene dihydrobromide were washed with methanol (15 mL) containing 2 drops of 48% HBr and ether (5 mL) and then dried (871 mg, 63%).

1′,8′-Dideoxy-1,2,3,4,5,6,7,8-octaethyl-*ac*-biladiene dihydrobromide (799 mg, 1.16 mmol) was divided into three equal portions. Each portion was added to a flask containing methanol (67 mL), 4-methylbenzaldehyde (559 mg, 4.65 mmol), and 10 drops of 48% aqueous HBr. Each mixture was heated to reflux for 48 h. The red-brown solutions were cooled to room temperature, combined, and slowly treated with $NaHCO_3$ (6 g) in water (30 mL). The solution was stirred for 30 min during which time a purple precipitate formed. This solid was worked up as described for **1**. The major dark red band from chromatography crystallized from CH_2Cl_2/CH_3OH as purple needles (529 mg, 73%). ^1H NMR ($CDCl_3$): H_{meso} 10.06 (s, 2 H), 9.81 (s, 1 H); aryl H_o 7.97 (d, 7.7 Hz, 2 H), H_m 7.36 (d, 7.4 Hz, 2 H); CH_2CH_3 4.05–3.85 (m, 12 H), 2.68 (q, 7.6 Hz, 4 H); $C_6H_4CH_3$ 2.63 (s, 3 H); CH_2CH_3 1.81 (t, 7.4 Hz, 12 H), 1.75 (t, 7.5 Hz, 6 H), 1.04 (t, 7.3 Hz, 6 H); NH −3.2 (d, 2 H). LSIMS (tetraglyme): m/e = 625 (cluster, M^+). UV–vis (CH_2Cl_2; λ_{max}, nm (log ε)): 406 (5.49), 504 (4.51), 536 (4.00), 572 (3.91).

[Re^{II}(AHEDMP)]$_2$ (3).[55] H_2AHEDMP (100 mg, 0.163 mmol), Re_2O_7 (90 mg, 0.186 mmol), phenol (500 mg), and a boiling stone were added to a test tube (1 × 15 cm), and the resultant mixture was heated to 210 °C with a silicone oil bath for 12 h. The phenol was then removed by sublimation under vacuum (50 °C, 0.01 Torr), and the dark green residue was dissolved in CH_2Cl_2 and flash chromatographed (SiO_2, 1 × 10 cm). A dark green band eluted with 3% methanolic CH_2Cl_2 and was evaporated. The residue was redissolved in CH_2Cl_2 and then treated with $(CH_3)_3SiCl$ (0.1 mL). The product, Re^V(AHEDMP)(O)(Cl), precipitated from this solution with the addition of hexanes (108 mg, 78%). LSIMS (tetraglyme): m/e = 849 (cluster, M^+), 813 (cluster, $M^+ - Cl$).

Re^V(AHEDMP)(O)(Cl) (100 mg, 0.118 mmol) and a boiling stone were added to a 50-mL conical flask equipped with a Teflon high-vacuum stopcock and an O-ring joint. PEt_3 (~12 mL) was then vacuum-transferred into the conical flask, and the mixture was degassed once with a freeze–pump–thaw procedure (0.01 Torr). The suspension was heated to boiling under an argon atmosphere for 12 h during which time it became homogeneous and a dark orange color. The solution was cooled to 25 °C, and then the excess PEt_3 was vacuum-transferred into another flask. The dark orange residue was heated under vacuum (80 °C, 0.01 Torr) for 8 h and then taken into the drybox. The toluene-soluble portion of this solid was flash chromatographed (SiO_2, 1 × 8 cm), eluting with the same solvent. The first orange band was collected and evaporated to yield Re^{II}(AHEDMP)$(PEt_3)_2$ as an orange solid (74 mg, 61%). LSIMS (tetraglyme): m/e = 1033 (cluster, M^+), 915 (cluster, $M^+ - PEt_3$), 797 (cluster, $M^+ - 2\ PEt_3$).

In the drybox, Re^{II}(AHEDMP)$(PEt_3)_2$ (52 mg, 0.052 mmol) was dissolved in benzene (5 mL) and the resultant solution added to a pyrolysis tube. The stopcock was sealed, and the tube was removed from

(47) (a) McLain, S. J. *J. Am. Chem. Soc.* **1988**, *110*, 643–644. (b) Amer, S.; Kramer, G.; Pöe, A. *J. Organomet. Chem.* **1981**, *209*, C28–C30. (c) Krause, J. R.; Bidinosti, D. R. *Can. J. Chem.* **1975**, *53*, 628–632.

(48) Tilset, M.; Parker, V. D. *J. Am. Chem. Soc.* **1989**, *111*, 6711–6717.

(49) Kegley, S. E.; Husk, G. R.; Brookhart, M. *Organometallics* **1982**, *1*, 760–762.

(50) Perrin, D. D.; Armarego, W. L. F.; Perrin, D. R. *Purification of Laboratory Chemicals*, 2nd ed.; Pergamon Press: New York, 1980; p 250.

(51) Van Geet, A. N. *Anal. Chem.* **1968**, *40*, 2227–2229.

(52) Program QCMP 059 from the Quantum Chemical Program Exchange, Department of Chemistry, Indiana University.

(53) (a) Johnson, A. W.; Kay, I. T. *J. Chem. Soc.* **1965**, 1620–1629. (b) Bonnett, R.; Buckley, D. G.; Hamzetash, D. *J. Chem. Soc., Perkin Trans. 1* **1981**, *1*, 322–325.

(54) Paine, J. B., III; Woodward, R. B.; Dolphin, D. *J. Org. Chem.* **1976**, *41*, 2826–2835.

(55) The tungsten and rhenium porphyrin syntheses are similar to those reported for the corresponding octaethylporphyrin and *meso*-tetraphenylporphyrin complexes.[5,56]

(56) Collman, J. P.; Garner, J. M.; Kim, K.; Ibers, J. A. *Inorg. Chem.* **1988**, *27*, 4513–4516.

the drybox. The dark orange solution was frozen with a liquid nitrogen bath and then warmed to 0 °C under vacuum (0.01 Torr) to sublime the benzene. The amorphous orange solid was then heated under high vacuum (210 °C, 10^{-5} Torr) for 12 h. The orange solid became blue-brown. The vacuum stopcock was sealed, and the tube was taken into the drybox. The loose solid was isolated from a small amount of orange sublimate to yield the $[Re^{II}(AHEDMP)]_2$ product (38 mg, 91%). ^1H NMR ($C_6D_5CD_3$, −25 °C): $H_{o'}$ 8.82 (d, 8.2 Hz, 1 H), $H_{m'}$ 7.54 (d, 7.2 Hz, 1 H), H_o 6.90 (d, 8.3 Hz, 1 H), H_m 6.72 (d, 7.7 Hz, 1 H); CH_2CH_3 4.25–3.95 (m, 4 H), 3.90–3.55 (overlapping m), 3.05–2.90 (m, 2 H), 2.60–2.40 (m, 2 H); CH_3 3.79 (overlapping s); OCH_3 3.63 (overlapping s); CH_2CH_3 1.62 (t, 6.7 Hz, 12 H), 1.29 (t, 6.0 Hz, 6 H). FABMS (sulfolane): m/e = 1594 (cluster, M^+).

$[Mo^{II}(TOEP)]_2$ (4).[57] In the drybox, H_2TOEP (77 mg, 0.0120 mmol), $Mo(CO)_4Cl_2$ (400 mg, 1.43 mmol), and 35 mL of toluene containing 1.5 mL of 2,6-lutidine were refluxed for 22 h. The solution was then evaporated to yield a dark purple solid. The toluene-soluble products were extracted from the residue and flash chromatographed (SiO_2, 2 × 15 cm, toluene). The first dark brown band was collected and evaporated. Recrystallization from toluene/octane produced 36 mg (20%) of brown powder. ^1H NMR (C_6D_6): H_{meso} 9.46 (s, 1 H), 9.29 (s, 2 H); $H_{o'}$ 10.07 (d, 10.5 Hz, 1 H), $H_{m'}$ 8.06 (d, 10.5 Hz, 1 H), H_o 7.00 (d, 10.5 Hz, 1 H), H_m 6.89 (d, 10.5 Hz, 1 H); CH_2CH_3 4.67–4.60 (m, 2 H), 4.59–4.36 (m, 4 H), 4.35–4.14 (m, 2 H), 4.00–3.78 (m, 4 H), 3.15–3.02 (m, 2 H), 2.94–2.81 (m, 2 H); CH_3 2.61 (s, 3 H); CH_2CH_3 1.76 (t, 7.5 Hz, 6 H), 1.62 (overlapping t, 12 H), 1.44 (t, 7.5 Hz, 6 H). FABMS (sulfolane): m/e = 1438 (cluster, M^+).

$[W^{II}(TOEP)]_2$ (5).[56] H_2TOEP (300 mg, 0.480 mmol), $W(CO)_6$ (500 mg, 1.42 mmol), and DMF (10 mL) containing octane (1 mL) were refluxed under nitrogen for 4 h. The solution was cooled and poured into a brine solution. The solid was vacuum filtered and washed with water (100 mL). The residue was redissolved in CH_2Cl_2, filtered, and evaporated to dryness to yield a greenish brown solid. This product was loaded on a flash chromatography column (SiO_2, 2 × 14 cm), and W^V(TOEP)(O)(OCH_3) was isolated as a crude solid (162 mg, 39%) similar to the procedure described for W(OEP)(O)(OCH_3).[5] LSIMS (tetraglyme): m/e = 823 (cluster, $M^+ - OCH_3$).

In the drybox, W^V(TOEP)(O)(OCH_3) (150 mg, 0.176 mmol) was added to a 15-mL conical flask equipped with a Teflon high-vacuum stopcock and O-ring joint. The solid was dissolved in CH_2Cl_2 (7 mL) and then treated with Si_2Cl_6 (94 mg, 0.35 mmol). The color rapidly changed from green to brown, and the solution was stirred for another 2 h. The solution was then evaporated to yield a brown-blue residue. In the same Schlenk flask, Al(Hg) (500 mg) and PEt_3 (2 mL) were added to this solid, the mixture was degassed once with a freeze–pump–thaw cycle (0.01 Torr), and the stopcock was sealed. Protected with a blast shield and a hood sash, the mixture was heated at 125 °C for 36 h.

Caution! Although no accidents have occurred utilizing this procedure, there exists the possibility of an explosion so the safety precautions above must be performed. Do not handle the reaction flask when the reaction solution is hot (≥30 °C). The solution volume must be less than half the flask volume so the vapor from the boiling solution has room to expand. In general, heating liquids such as triethylphosphine above their boiling points in sealed glassware is extremely dangerous and should not be performed routinely. It is only done here to minimize the hydrolysis of an intermediate which is presumably formed in the previous reaction. The sonication procedure below should only be performed after the reaction mixture has cooled to room temperature. The flask can then be safely transferred to a sonicator located in the hood, keeping the safety shield between the flask and researcher at all times during the transfer and sonication. A long-sleeved labcoat and Kevlar or leather gloves inside gauntlet neoprene gloves should be worn while handling the reaction flask.

The mixture was cooled at the 12- and 24-h intervals and sonicated briefly to facilitate dissolution. The mixture became a dark orange color. After the 36-h period had ended, the solution was cooled and the excess PEt_3 vacuum-transferred into another flask. The dark brown-orange residue was then heated under vacuum (60 °C, 0.01 Torr) for 5 h and taken into the drybox. The toluene-soluble products were extracted from the residue and flash chromatographed (SiO_2, 2 × 8 cm, toluene). The first orange band was collected and evaporated to yield an air-sensitive solid (65 mg).

In the drybox, the orange solid was dissolved in benzene (3 mL) and the resultant solution added to a vacuum pyrolysis tube. The sealed tube was removed from the drybox, quickly frozen with a liquid nitrogen bath, and then evacuated (0.01 Torr). The solid solution was warmed to 0 °C under vacuum and the benzene sublimed away to yield an amorphous orange powder. This solid was heated under vacuum (200 °C, 10^{-6} Torr) for 48 h. The pyrolysis tube was sealed to protect the solid product from oxygen, isolated from the vacuum manifold, and then taken into the drybox. The brown-blue product was dissolved in toluene and flash chromatographed (SiO_2, 1 × 5 cm), eluting with the same solvent. The first brown band was collected and evaporated to yield the dark brown solid product $[W^{II}(TOEP)]_2$ (31 mg, 62%). ^1H NMR ($C_6D_5CD_3$, 50 °C): H_{meso} 8.80 (s, 1 H), 8.50 (s, 2 H); $H_{o'}$ 9.57 (d, 1 H), $H_{m'}$ 7.91 (d, 1 H), H_o and H_m overlap with protio toluene peaks; CH_2CH_3 4.22, 3.78, 2.95, 2.63 (m); $C_6H_4CH_3$ 2.59 (s, 3 H); CH_2CH_3 1.64 (t, 12 H), 1.29 (t, 12 H). FABMS (sulfolane): m/e = 1613 (cluster, M^+).

The tungsten dimer contained a minor impurity which could not be eliminated by column chromatography. Although the identity of this impurity is unknown, it may be the oxide, W(TOEP)(O), which was detected in the mass spectroscopy of $[W(TOEP)]_2$ (the dimers are acutely oxygen sensitive). The lineshapes of the impurity ^1H NMR resonances show insignificant broadening or sharpening between −80 and +80 °C, suggesting no interaction with $[W(TOEP)]_2$.

$[Ru^{II}(TOEP)]_2$ (6).[58] H_2TOEP (30 mg, 0.048 mmol) and $Ru_3(CO)_{12}$ (30 mg, 0.047 mmol) were heated at reflux for 3 h in 1,2-dichlorobenzene (20 mL) under CO. The solvent was removed under reduced pressure; the residue was dissolved in toluene, loaded on a flash chromatography column (SiO_2, 2 × 15 cm), and eluted with toluene. The first red band was collected and the product, Ru^{II}(TOEP)(CO)(CH_3OH), recrystallized from CH_2Cl_2/MeOH (33 mg, 88%). ^1H NMR ($CDCl_3$): H_{meso} 9.97 (s, 2 H), 9.89 (s, 1 H); H_o 8.04 (d, 2 H), H_m 7.44 (d, 2 H); CH_2CH_3 4.1–3.85 (m, 12 H); CH_3 2.72 (s, 3 H); CH_2CH_3 2.70 (q, 4 H); CH_2CH_3 1.93 (overlapping t, 18 H), 1.21 (t, 6 H). UV/vis (CH_2Cl_2; λ_{max}, nm (log ε)): 398 (5.04), 520 (4.35), 550 (4.45).

A solution of Ru^{II}(TOEP)(CO)(CH_3OH) (33 mg, 0.042 mmol) dissolved in pyridine (60 mL) was evacuated with three freeze–pump–thaw cycles and then irradiated with a high-pressure Hanovia Hg arc lamp for 3 h. The reaction solution was again evacuated with two freeze–pump–thaw cycles and irradiated for another 5 h. This later procedure was repeated and the solution transferred to the drybox. After the solvent was removed under vacuum, the residue was dissolved in THF and flash chromatographed (alumina, 1 × 15 cm), eluting with THF. The brown-orange eluant was evaporated and dried under vacuum (22 mg, 60%). ^1H NMR (C_6D_6, 23 °C): H_{meso} 9.65 (s, 1 H), 9.63 (s, 2 H); H_o 8.16 (d, 2 H), H_m 7.27 (d, 2 H); pyr-H_p 4.7 (t, 2 H); pyr-H_m 4.18 (t, 2 H); CH_2CH_3 3.9–3.7 (overlapping q, 12 H), CH_2CH_3 2.82 (q, 4 H); CH_3 2.42 (s, 3 H); pyr-H_o 2.37 (d, 4 H); CH_2CH_3 1.95–1.82 (overlapping t, 18 H); CH_2CH_3 1.38 (t, 6 H). UV/vis (CH_2Cl_2; λ_{max}, nm): 362 (sh), 398 (Soret), 452 (br), 498, 524.

In the drybox, $Ru^{II}(TOEP)(NC_5H_5)_2$ (20 mg, 0.023 mmol) was dissolved in benzene (5 mL) and the resultant solution added to a vacuum pyrolysis tube. The sealed tube was removed from the drybox, quickly frozen with a liquid nitrogen bath, and then evacuated (0.01 Torr). The solid solution was warmed to 0 °C under vacuum and the benzene sublimed away to yield an amorphous powder. This solid was heated under vacuum (180 °C, 10^{-6} Torr) for 13 h. The pyrolysis tube was sealed to protect the solid product from oxygen, isolated from the vacuum manifold, and then taken into the drybox. The product, $[Ru^{II}(TOEP)]_2$ (15 mg, 92%), was transferred to a sealed NMR tube. ^1H NMR (C_6D_6, 19 °C): CH_2CH_3 26.79, 25.21, 24.87, 21.94, 17.06, 11.15, 9.62, 8.57 (br s, 4 H each); H_{meso} 14.37 (s, 2 H), 7.04 (s, 4 H); tolyl-H 12.31, 8.88, 6.90, 5.50 (s, 2 H each); tolyl-CH_3 3.35 (s, 6 H); CH_2CH_3 4.24, 2.98, 2.89, 2.61 (t, 12 H each).

Acknowledgment. We thank the National Science Foundation (Grant CHE88-14149) for providing funding for the experimental work and NMR instruments used in this study. We thank the Mass Spectrometry Facility, University of California, San Francisco, supported by the NIH Division of Research Resources, Grant RR 01614. J.M.G's portion of this work is dedicated to his father, James H. Garner.

Registry No. 1, 138235-67-3; **2**, 65858-40-4; **3**, 122676-04-4; **4**, 138259-25-3; **5**, 138259-26-4; **6**, 138259-30-0; Re(AHEDMP)(O)(Cl), 138259-27-5; Re(AHEDMP)(PEt_3)$_2$, 138259-28-6; W(TOEP)(O)(OCH_3), 138259-29-7; Ru(TOEP)(CO)(CH_3OH), 138259-31-1; Ru(TOEP)(NC_5H_5)$_2$, 138259-32-2; 1′,8′-dideoxy-1,2,3,4,5,6,7,8-octaethyl-*ac*-biladiene dihydrobromide, 1182-50-9.

(57) The $[Mo(TOEP)]_2$ synthesis is similar to that reported for *meso*-substituted molybdenum–octaethylporphyrin dimers.[4]

(58) The synthesis of $[Ru(TOEP)]_2$ is analogous to that reported for $[Ru(OEP)]_2$.[14]